Synthesis, Photophysics and Nonlinear Optical Properties of Stilbenoid Pyrimidine-Based Dyes Bearing Methylenepyran Donor Groups

ARTICLE *in* CHEMPHYSCHEM · AUGUST 2013

Impact Factor: 3.42 · DOI: 10.1002/cphc.201300419 · Source: PubMed

10 AUTHORS, INCLUDING:

Sylvain Achelle
Université de Rennes 1
48 PUBLICATIONS **526** CITATIONS
SEE PROFILE

Jean-Pierre Malval
Université de Haute-Alsace
74 PUBLICATIONS **630** CITATIONS
SEE PROFILE

L. Mager
French National Centre for Scientific Resea…
81 PUBLICATIONS **499** CITATIONS
SEE PROFILE

Jean-Luc Fillaut
Université de Rennes 1
85 PUBLICATIONS **1,525** CITATIONS
SEE PROFILE

ChemPubSoc Europe

ARTICLES

Let's get (photo)physical! The nonlinear properties and the photophysical behavior of a series of π-conjugated chromophores that incorporate an electron-deficient pyrimidine core (A) and γ-methylenepyrans as terminal donor (D) groups are thoroughly investigated.

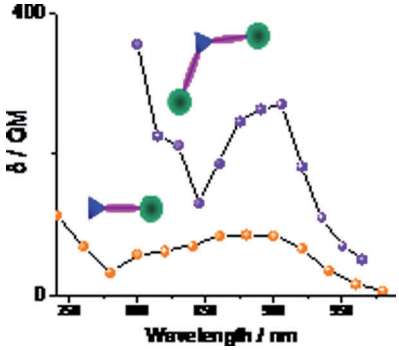

S. Achelle, J.-P. Malval,* S. Aloïse, A. Barsella, A. Spangenberg, L. Mager, H. Akdas-Kilig, J.-L. Fillaut, B. Caro, F. Robin-le Guen*

■■ – ■■

Synthesis, Photophysics and Nonlinear Optical Properties of Stilbenoid Pyrimidine-Based Dyes Bearing Methylenepyran Donor Groups

DOI: 10.1002/cphc.201300419

Synthesis, Photophysics and Nonlinear Optical Properties of Stilbenoid Pyrimidine-Based Dyes Bearing Methylenepyran Donor Groups

Sylvain Achelle,*[a] Jean-Pierre Malval,*[b] Stéphane Aloïse,[c] Alberto Barsella,[d] Arnaud Spangenberg,[b] Loic Mager,[d] Huriye Akdas-Kilig,[e] Jean-Luc Fillaut,[e] Bertrand Caro,[a] and Françoise Robin-le Guen[a]

The nonlinear properties and the photophysical behavior of two π-conjugated chromophores that incorporate an electron-deficient pyrimidine core (A) and γ-methylenepyrans as terminal donor (D) groups have been thoroughly investigated. Both dipolar and quadrupolar branching strategies are explored and rationalized on the basis of the Frenkel exciton model. Even though a cooperative effect is clearly observed if the dimensionality is increased, the nonlinear optical (NLO) response of this series is moderate if one considers the nature of the D/A couple and the size of the chromophores (as measured by the number of π electrons). This effect was attributed to a disruption in the electronic conjugation within the dyes' scaffold for which the geometry deviates from planarity owing to a noticeable twisting of the pyranylidene end-groups. This latter structural parameter also has a strong influence on the excited-state dynamics, which leads to a very efficient fluorescence quenching.

1. Introduction

In recent years, there has been a rapid progress in the development of nonlinear optical (NLO) materials, which owes to their great impact and promising potentials in a wide range of applications such as multiphoton microscopy,[1] photodynamic therapy,[2] optical limiting,[3] multiphoton fabrication[4] and high density optical data storage.[5] A fundamental issue that constitutes the cornerstone of all these applications concerns the elaboration of valuable design strategies to tune the NLO response of the materials in a methodical manner. Some key principles and structure–property relationships have been clearly identified especially for organic materials.[6] One of the simplest integrated systems consists of an electron-donor (D) and an electron-acceptor (A) group that are connected together by using a π-conjugated bridge as an "electron relay". Within this prototypal dipolar configuration, several parameters account for the choice of the central π-conjugated fragment: 1) the nature of linkers (double vs triple bonds),[7] 2) the size of the bridge as measured by the number of π electrons,[8] 3) the donor or acceptor character of the bridge, 4) the inherent rigidity or flexibility of the bridge and 5) the aromatic character of the bridge. Several π-spacers have been successfully employed, examples are: phenylene-vinylene,[9] phenylene-ethynylene,[7] fluorene,[10] dithienothiophene[11] and porphyrin.[12] A second fruitful strategy involves an increase in the dimensionality of the molecule with a recursive implementation of several D-π-A chromophores into a multibanched configuration[13] present in quadrupoles,[9b,14] octupoles[13,14c,15] or dendrimers.[16] Owing to a cooperative interaction among each arm, the magnitude of the resulting NLO response is found to be much greater than the sum of the discrete NLO responses.

In line with this branching strategy, this paper presents the photophysical feature of two chromophores that result from the molecular association of a new D/A couple linked by flexible phenylene-vinylene bridges (Scheme 1). The acceptor subunit is a substituted pyrimidine ring (1,3-diazine) that has been extensively used as a building block for the synthesis of functionalized π-conjugated NLO materials.[17] The structural shape

[a] Dr. S. Achelle, Prof. B. Caro, Prof. F. Robin-le Guen
Institut des Sciences Chimiques de Rennes
UMR CNRS 6226, IUT de Lannion
rue Edouard Branly, BP 30219
22302 Lannion Cedex (France)
E-mail: sylvain.achelle@univ-rennes1.fr

[b] Dr. J.-P. Malval, Dr. A. Spangenberg
Institut de Science des Matériaux de Mulhouse
UMR CNRS 7361, Université de Haute-Alsace
15 rue Jean Starcky ,68057 Mulhouse (France)
E-mail: jean-pierre.malval@uha.fr

[c] Dr. S. Aloïse
Laboratoire de Spectrochimie Infrarouge et Raman
UMR CNRS 8516
Université des Sciences et Technologies de Lille
59655 Villeneuve d'Ascq Cedex (France)

[d] Dr. A. Barsella, Dr. L. Mager
Département d'Optique ultra-rapide et Nanophotonique
IPCMS-CNRS 23 Rue du Loess, BP 43
67034 Strasbourg Cedex 2 (France)

[e] Dr. H. Akdas-Kilig, Dr. J.-L. Fillaut
Institut des Sciences Chimiques de Rennes UMR CNRS 6226
Campus de Beaulieu, 263 av. du Général Leclerc
35042 Rennes (France)

Supporting information for this article is available on the WWW under http://dx.doi.org/10.1002/cphc.201300419.

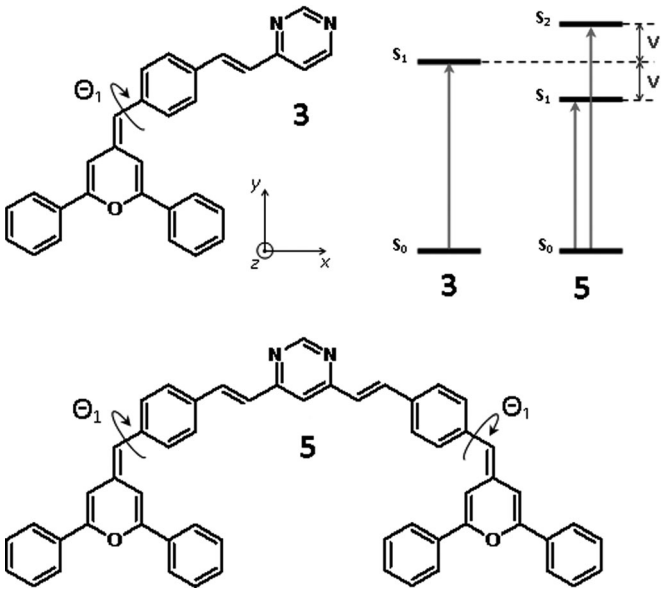

Scheme 1. Molecular structures of chromophores. Representation of the effects of the interbranch coupling on the electronic levels on going from **3** to **5**.

of the investigated pyrimidines gives rise to either one-dimensional or two-dimensional D-π-A or D-π-A-π-D type molecules, respectively. The donor terminal group is a γ-methylenepyran system, which is considered as a "proaromatic" donor[18] because it gains aromaticity through a charge transfer process. This effect influences the degree of mixing between the quinoidal and zwitterionic limiting resonance forms of the ground state. As previously emphasized[19] the NLO properties are directly connected to the optimization of this latter degree of mixing. In the present contribution, we show that the twist angle within stilbenoid pyrimidine-based dyes bearing methylenpyran donor groups has a strong influence on the NLO properties but also drives the major relaxation process at excited state in this series.

2. Results and Discussion

2.1 Synthesis

The linear push-pull compound **3** has been obtained in two steps from readily available 4-methylpyrimidine (Scheme 2). The first step consists of a condensation reaction between 4-methylpyrimidine and 4-(diethoxymethyl)benzaldehyde in boiling aqueous NaOH (5 M) by using Aliquat 336 as a phase-transfer catalyst. This is followed by deprotection of the acetal group in acidic media, which leads to compound **1** according to the procedure initially described by Vanden Eynde.[20] The second step consists of a Wittig reaction between aldehyde **1** and phosphonium salt **2**[21], which leads to compound **3**.[22] Quadrupolar derivative **5** has been obtained by the same synthetic procedure that starts from 4,6-dimethylpyrimidine (Scheme 3). These materials are perfectly stable in the solid

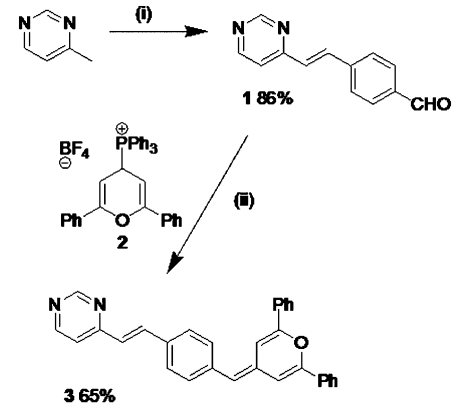

Scheme 2. Reaction scheme for the formation of **3**. i) 4-(diethoxymethyl)-benzaldehyde, Aliquat 336, aqeous NaOH (5 M), 2 h, Δ then HCl, acetone, 5 min at room temperature ii) *n*BuLi, THF, 2 h, $T = -78\,^{\circ}C \rightarrow RT$.

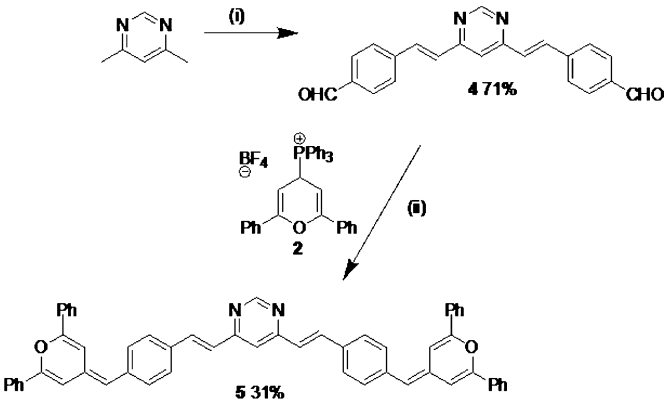

Scheme 3. Reaction scheme for the formation of **5**. i) 4-(diethoxymethyl)-benzaldehyde, Aliquat 336, aqeous NaOH (5 M), 2 h, Δ then HCl, acetone, 5 min at room temperature ii) *n*BuLi, THF, 2 h, $-78\,^{\circ}C \rightarrow RT$.

state and can be stored without the need for special precautions.

2.2 Electronic and Linear Absorption Properties of the Ground State

Figure 1 shows the absorption spectra of **3** and **5** in dichloromethane. Both dyes exhibit three absorption peaks at approximately $\lambda = 255$, 290 and > 400 nm. Notably, a slight shoulder located at the blue edge of the longest wavelength absorption band is observed for compound **5**. The UV absorption band at $\lambda = 255$ nm should be attributed to the presence of the ^1L_a and ^1L_b electronic transitions centered on the 4-methylene-4*H*-pyran moiety.[23] Interestingly, this band is 2-fold intensive for the two-arm chromophore as compared to the dipolar one. Such a linear correlation first indicates that, for chromophore **5**, no intramolecular interaction at the ground state occurs between the pyranylydene groups, and the electronic conjugation between the 4-methylenepyran and the pyrimidine-based fragments remains comparable to that observed for **3** despite

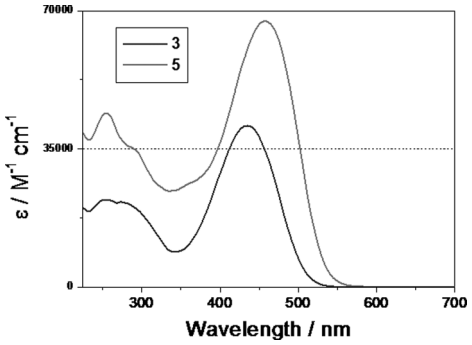

Figure 1. Absorption spectra of derivatives in dichloromethane.

the increase in dimensionality for the V-shaped structure. The fully optimized structures calculated at density functional theory (DFT) level are presented in Figure 2. Both dyes show quite similar geometries. The 4-methylenepyran and the 4-styrylpyrimidine fragments adopt a quasi-planar conformation but are twisted between each other, which leads to a torsional angle (Θ_1 in Scheme 1) of approximately 28°. Such a twisted geometry is independent of the substitution effects on the pyrimidine core. Moreover, increasing the 2-dimensionality on going from a 4-(styryl) to a 4,6-bis(styryl)pyrimidine subunit hardly affects the planarity observed between the pyrimidine and its styryl substituents, which results in hyperchromic and bathochromic effects. The longest wavelength absorption band that should encompass several π–π^* electronic transitions partially localized on the substituted pyrimidine moiety shifts to the low energy side of the spectrum and undergoes a 1.65-fold increase in intensity with ε_{max} of approximately 40900 $M^{-1}cm^{-1}$ and 67400 $M^{-1}cm^{-1}$ for compounds **3** and **5**, respectively.

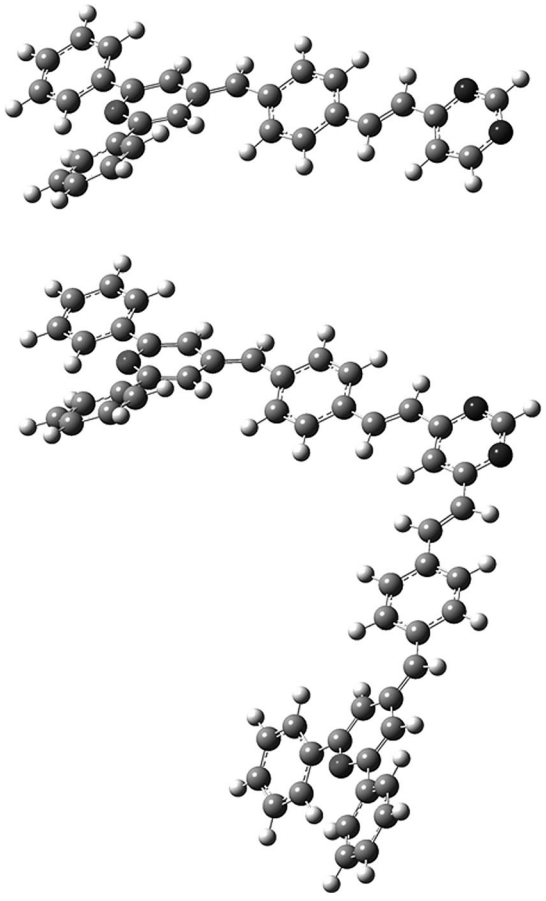

Figure 2. Optimized geometry of chromophores (PBE0/6-31G(d) level).

Figure 3 displays the cyclic voltamogramms of the derivatives in dichloromethane. Each compound exhibits an irreversible electrochemical oxidation wave with peaks at 0.73 V and 0.78 V versus the saturated calomel electrode (SCE) for **3** and **5**, respectively. These anodic potentials should be attributed to the oxidation of the methylenepyran group that probably leads to the formation of dimer byproducts as previously observed for similar derivatives.[22,24] Interestingly, the oxidation potentials of both compounds are quite comparable. This effect should be connected to the equivalent degree of electronic conjugation between the pyran and styrylpyrimidine subunits within both chromophores, which is consistent with the equivalent twisted geometries derived from DFT calculations. It was previously established that the oxidation potential of the methylenepyran group is strongly sensitive to the substituent on the exocyclic C=C bond. For instance, with a phenyl substituent, E_{ox} is approximately 0.73 V versus the SCE, and strongly increases to 1.03 V versus the SCE with a 4-pyridyl group.[25] Therefore, the oxidation potentials obtained for **3** and **5** highlight the low communication between the two heterocycle parts of the molecules.

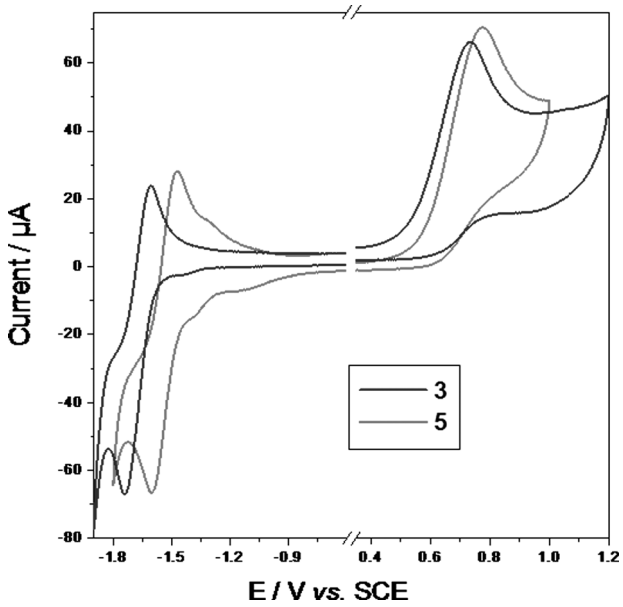

Figure 3. Cyclic voltamogramms of **3** and **5** in dichloromethane and $(n\text{Bu})_4NPF_6$ (0.1 M) on a platinum electrode at 200 mV s^{-1} (concentrations within mM range).

The cathodic part of both voltamogramms shows a quasi reversible reduction wave with a half-wave potential of approxi-

mately −1.68 V versus the SCE for **3** and −1.53 V versus the SCE for **5**. This reduction wave corresponds to the formation of a radical anion located on the pyrimidine moiety. It is strongly shifted to the high potential region with respect to that of the pyrimidine (i.e. −2.56 V vs the SCE).[26] Such an electrochemical effect was previously observed for 4,6-dithienyl or 4,6-diarylpyrimidine derivatives[26,27] and should be attributed to an efficient stabilization of the generated radical anion, which owes to a charge delocalization along the styryl branches. The extending charge delocalization within the multibranched chromophore **5** stabilizes the radical anion all the more, and leads to a further increase in the reduction potential (i.e. +150 mV) with respect to that of **3**.

Figure 4 shows the steady-state excitation anisotropies of **3** and **5** along with their respective absorption and fluorescence spectra recorded in a glassy matrix of 2-methyl tetrahydrofuran (2 MTHF). The calculated absorption spectra by using a time-dependent density functional theory (TD-DFT) method are also displayed on top of each experimental spectrum. The electronic distributions of the frontier orbitals are shown in Figure 5. The calculated energies of the electronic $S_0 \rightarrow S_n$ transitions and the experimental values of the 0–0 transition energies (E_{00}) are reported in Table 1. The vertical $S_0 \rightarrow S_1$ transition energies agree well with the experimental E_{00} values; these are measured from the intercept of the normalized absorption and fluorescence spectra recorded at $T = 77$ K in a glassy matrix of 2MTHF. In the case of **3**, the constant anisotropy within the long wavelength absorption band (410–530 nm) is consistent with the presence of a single electronic transition. The calculations indicate that this $S_0 \rightarrow S_1$ transition is a pure HOMO–LUMO transition with a high oscillator strength ($f > 1$). This transition implies some delocalization of charge all along the chromophore with a pronounced localization on the donor group (methylenepyran) in the HOMO and on the pyrimidine acceptor in the LUMO. Below $\lambda_{exc} \approx 400$ nm, the anisotropy strongly decreases, which suggests the presence of other electronic transitions with distinctive electronic symmetries.

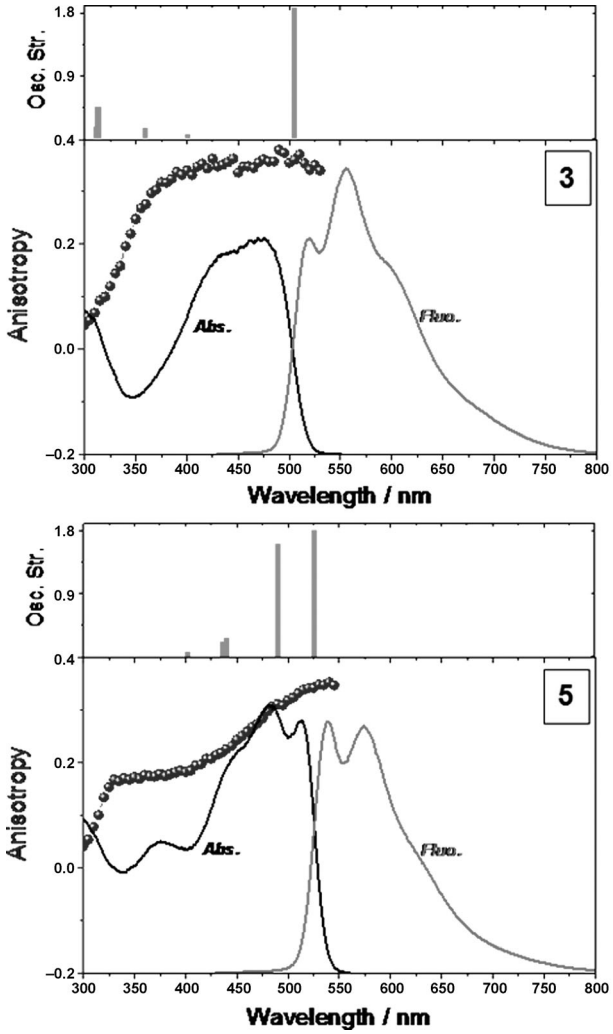

Figure 4. Top) Positions of vertical energy transitions along with corresponding electronic oscillator strengths calculated from the TDDFT method for both **3** and **5**. Bottom) Normalized absorption and fluorescence spectra (full lines) of chromophores in glassy matrix of 2-MTHF ($T = 77$ K). Excitation anisotropy spectra (circles) in glassy matrix of 2-MTHF ($T = 77$ K) for both **3** and **5**.

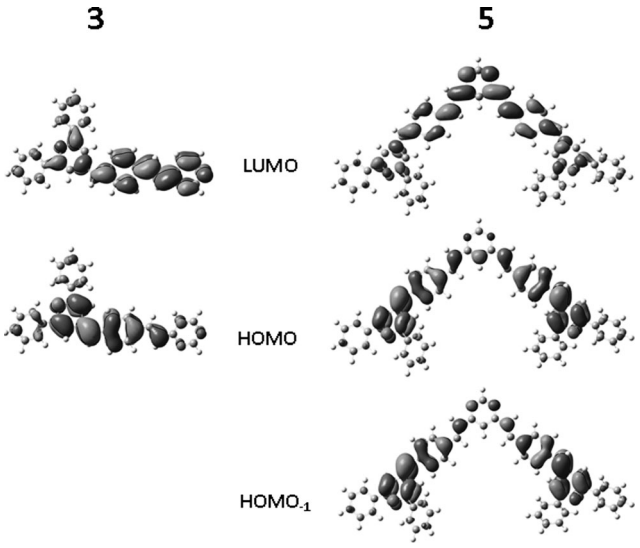

Figure 5. Representation of the molecular orbitals involved in the lowest energy electronic transitions of chromophores **3** and **5**.

The evolution of the excitation anisotropy spectrum of **5** is less straightforward. On going from $\lambda = 545$ to 480 nm, the anisotropy decreases sequentially from two narrow plateaus, then undergoes a strong drop below $\lambda = 475$ nm and remains constant in the $\lambda = 400$–330 nm range. These changes in the anisotropy spectrum are consistent with TD-DFT calculations, which predict the occurrence of two energetically close and strongly allowed transitions that dominate the longest wavelength absorption band. The $S_0 \rightarrow S_1$ transition mainly corresponds to the HOMO–LUMO (73%) transition, whereas the $S_0 \rightarrow S_2$ transition implies a major contribution (70%) from the HOMO$_{-1}$-LUMO (see Figure 5 for orbital symmetry). Both transitions clearly correspond to conjugated π–π* transitions and exhibit a charge

Table 1. TDDFT and experimental electronic transitions of chromophores.

Transition	3 Experimental E_{00} [eV]	Theoretical E_{th} [eV]	f	Pol.[a]	Major natural transitions (fractions)	5 Experimental E_{00} [eV]	Theoretical E_{th} [eV]	f	Pol.[a]	Major natural transitions (fractions)
$S_0 \rightarrow S_1$	2.47	2.46	1.872	$\underline{x},y$[b]	H-L	2.36	2.37	1.803	y	H-L (0.73), H_{-1}-L_{+1} (0.27)
$S_0 \rightarrow S_2$		3.09	0.064	$x,\underline{y}$[b]	H_{-1}-L (0.54), H_{-1}-L_{+1} (0.46)		2.53	1.598	x	H-L_{+1} (0.30), H_{-1}-L (0.70)
$S_0 \rightarrow S_3$		3.45	0.144	$x,\underline{y}$[b]	H_{-1}-L_{+1}(0.46), H-L_{+2} (0.54)		2.82	0.258	x	H_{-1}-L (0.31), H-L_{+1} (0.69)
$S_0 \rightarrow S_4$		3.96	0.455	X	H_{-2}-L (0.20), H_{-1}-L (0.80)		2.84	0.211	y	H-L (0.27), H_{-1}-L_{+1} (0.73)
$S_0 \rightarrow S_5$		3.99	0.160	y	H_{-2}-L (0.69), H_{-1}-L (0.18)[c]		3.08	0.067	x,z	H_{-1}-L_{+3} (0.27), H-L_{+3} (0.27) [c]
$S_0 \rightarrow S_6$		4.01	0.002	z	H_{-3}-L (0.64), H_{-3}-L_{+1} (0.19) [c]		3.09	0.051	x,z	H-L_{+4} (0.18), H_{-1}-L_{+4} (0.19) [c]

[a] Orientation of transition dipole. *xyz* axis are displayed in Scheme 1. [b] The main component is underlined. [c] The two principal natural transitions are displayed.

transfer from the periphery (pyran fragments) to the core (pyrimidine ring) of the dye.

The occurrence of these two transitions is well predicted within the framework of the Frenkel exciton model.[13,28] For a two-branched V-shaped chromophore, it is assumed that interbranch electrostatic interactions lead to the splitting of the one-exciton transition relative to the molecular synthon.[29] This twofold degeneracy occurs symmetrically for a homo-dimeric chromophore (see inset of Scheme 1) and leads to a S_1–S_2 gap of $2V$ in which V denotes the interbranch coupling. Such a symmetrical splitting is well-reproduced here: calculations show that the midpoint energy between the S_1 (2.37 eV) and S_2 (2.53 eV) levels of chromophore **5** matches the S_1 energy of **3** (i.e. 2.46 eV). The interbranch coupling can be estimated at approximately $E = 0.09$ eV. This value is moderate with respect to interbranch couplings calculated in the $E = 0.15$–0.20 eV range for symmetrical V-shaped structures that bear strong electron-withdrawing groups.[14c,d,15a] This moderate coupling should indicate a weak dipole moment change upon dye excitation from the ground to Franck–Condon states. In the high-energy region (i.e. $\lambda_{exc} < 475$ nm), two sets of two close-lying transitions are predicted. The first set (namely $S_0 \rightarrow S_3$ and $S_0 \rightarrow S_4$) is positioned within the region that corresponds to the strong change of the anisotropy spectrum. This latter effect should be attributed to an important change in the relative orientation of the transition dipole moments associated with each transition (see Table 1). Interestingly, the second set of $S_0 \rightarrow S_n$ transitions located at approximately $\lambda = 400$ nm are weakly allowed ($f < 0.1$) but exhibit similar electronic polarizations in line with the constant anisotropy observed in this spectral region.

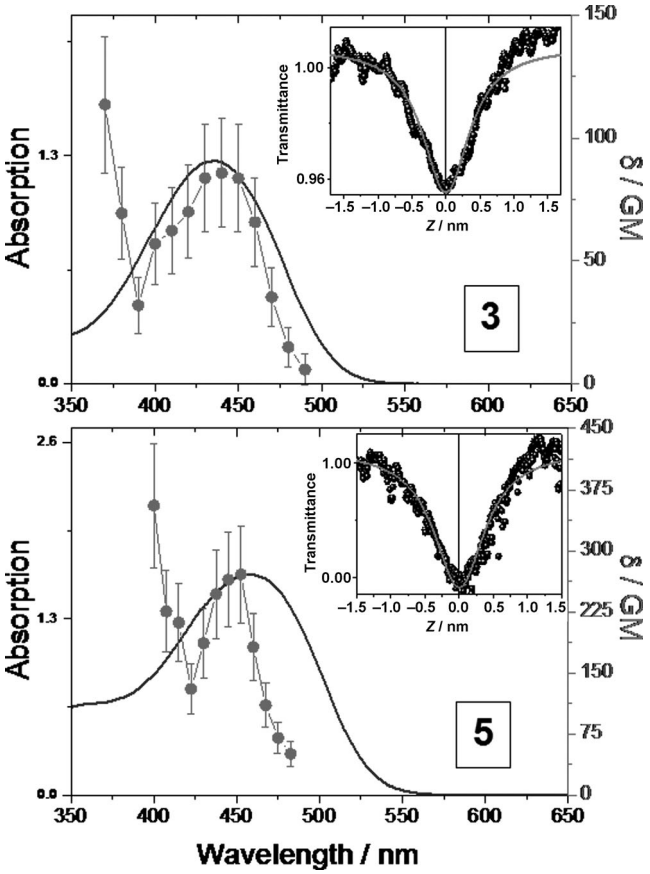

Figure 6. One- (full lines) and two- (data points) photon absorption spectra of dyes in dichloromethane for **3** and **5**. (The 2PA spectra are plotted against half the excitation wavelength). Inset: Typical *Z*-Scan graph and its best fitting curve (see text).

2.3 Two-Photon Absorption Properties

The two-photon absorption spectra have been measured in the $\lambda = 740$–980 nm range by using the open aperture *Z*-scan technique.[30] The one- (1PA) and two-photon (2PA) absorption spectra of the compounds are shown in Figure 6. The 2PA bands are plotted against half the excitation wavelength to have a direct comparison with the linear absorption spectra. According to our spectral resolution, it appears that the lowest energy 2PA band of **3** reasonably matches that of its 1PA one and shows a maximum 2PA cross-section (δ) of 86 ± 9 GM at $\lambda = 880$ nm. Despite the strong electron-withdrawing character of the pyrimidine core and the good electron-donating ability of the pyran group for which the oxidation potential is equivalent to that of a *N*,*N*′-dimethylaniline group (0.78 V vs SCE),[31] the δ_{max} value obtained for **3** is relatively weak with respect to 2PA cross-sections of other linear "push-pull" stilbenoid systems. For instance, 4-dialkylamino-4′-nitrostilbene[32] or 4-

alkoxy-4′-nitrostibene[4f] exhibit a δ_{max} of approximately 191 GM and 180 GM, respectively. Cui et al.[33] reported that an electron-deficient triazine core connected by a vinylene linker to a dimethylaniline group leads to a δ_{max} of 340 GM. In addition, if we normalize the 2PA cross-section by the effective number of π electrons (N_e) as proposed by Kuzyk et al.[8] the weak 2PA ability of **3** becomes even more sizeable because the ratio δ/N_e drops to 2.7 for **3**, which is 5 times lower than the δ/N_e values for the other cited stilbenes.

We assume that the flexible single bond that connects the stilbenyl moiety to the terminal donor group noticeably affects the nonlinear absorption properties of our derivatives. The flexible rotation between the donor and acceptor subunits (i.e. Θ_1 in Scheme 1) does not guarantee an optimum planar geometry that should maximize the π-orbital overlap. Such an influence of the twisted geometry on the 2PA cross-section was rationalized by Ahn et al.[12a] for a series of *meso*-linked porphyrin dimers that exhibit a gradual increase in the twist angle between the two porphyrins. On going from a near planar to perpendicular structure, the 2PA cross-section collapses by a factor of 75. As shown in Figure 6, the 2PA maximum of the two-branched chromophore **5** is blueshifted with respect to twice its linear absorption maximum. This should be attributed to the near centrosymmetry of the D-π-A-π-D dye, which leads theoretically to a two-photon forbidden $S_0 \rightarrow S_1$ transition. The longest wavelength 2PA band of **5** shows a maximum located at approximately $\lambda = 900$ nm with δ_{max} of 271 ± 28 GM, which leads to δ/N_e of approximately 4.7. Therefore, a cooperative enhancement of the 2PA efficiency is clearly evidenced on going from a one-dimensional D-π-A system to a quadrupolar branching structure.

2.4 Second-Order Nonlinear Measurements

Second-order nonlinear properties have been studied in $CHCl_3$ solution by using the electric-field-induced second-harmonic generation technique (EFISHG), which provides information about the scalar product $\mu\beta$ (2ω) of the vector component of the first hyperpolarisability tensor β and the dipole moment vector.[34] This product is derived according to Equation (1) taking into consideration that $\gamma_0(-2\omega,\omega,\omega,0)$, the third-order term, is negligible for the push-pull compounds under study. This approximation is usually used for push-pull organic and organometallic molecules.

$$\gamma_{EFISH} = \mu\beta/5kT + \gamma_0(-2\omega,\omega,\omega,0) \quad (1)$$

Measurements are performed at $\lambda = 1907$ nm, and obtained from a Raman-shifted Nd:YAG^+ laser source, which allowed us to work far from the resonance peaks of the compounds we investigated (**3** and **5**). $\mu\beta$ values of 400 and 770 10^{-48} esu were obtained respectively for compounds **3** and **5**. The $\mu\beta$ values of the two compounds are positive, which indicates that the excited states are more polarized than the ground states ($\mu e > \mu g$). In addition, this implies that the ground and excited states are polarized in the same direction. The positive values are in accordance with the emission solvatochromism observed for the compounds (see later). The $\mu\beta$ value obtained for compound **3** is higher than the value obtained for a 4-styrylpyrimidine substituted by a dimethylamino group (330 10^{-48} esu).[17b] Notably, the D-π-A-π-D dye **5** is not completely symmetric, and this has been shown on the DFT-optimized geometry. This compound exhibit a higher $\mu\beta$ value than the dipolar compound **3**.

2.5 Excited-States Properties

Both chromophores are nonfluorescent in apolar and low polar solvents (e.g. hexane or ethyl ether) at room temperature, and are weakly emissive if the solvent polarity is increased (Table 2). **5** is more emissive than **3**. In dichloromethane, the fluorescence quantum yield (Φ_f) is approximately 10^{-3} for **3** and 2.5×10^{-3} for **5**. In both cases, the structureless fluorescence band is very broad (full width at half maximal (FWHM) ≈ 4500 cm^{-1}) and is located in the $\lambda = 450$–800 nm range (Figure S1 in the Supporting Information). **3** and **5** clearly exhibit strong Stokes shifts ($\Delta\upsilon_{ST}$), which increase with solvent polarity. The fluorescence spectra undergo a pronounced bathochromic effect, whereas only a small solvent-induced shift is observed for the absorption bands upon an increase in the solvent polarity. This provides clear evidence for a significant electronic and/or geometrical change between ground and emitting states.

Table 2. Spectroscopic data of the ground and excited states of compounds in various solvents.

Solvent[a]	**3** λ_a [nm]	λ_f [nm]	FWHM[b] [cm^{-1}]	$\Phi_f \times 10^2$	Stokes Shift [cm^{-1}]	**5** λ_a [nm]	λ_f [nm]	FWHM[a] [cm^{-1}]	$\Phi_f \times 10^2$	Stokes Shift [cm^{-1}]
ETA	425	546	4690	0.04	5214	446	568	4145	0.12	4816
2MTHF	428	557	4840	0.04	5411	450	576	4334	0.13	4861
THF	431	556	4982	0.06	5216	452	577	4190	0.17	4793
DCM	436	566	4675	0.10	5268	458	609	4095	0.22	5414
ACT	427	581	4260	0.09	6207	447	630	4040	0.19	6498
DMF	434	592	4505	0.19	6150	456	652	4020	0.28	6592

[a] Solvents are: ETA = ethyl acetate, 2MTF = 2-methyltetrahydrofuran, THF = tetrahydrofuran, DCM = dichloromethane, ACT = acetone and DMF = dimethylformamide. [b] Full width at half maximum for fluorescence bands.

The dipole moment change ($\Delta\mu_{ge}$) between ground and excited states can be estimated by using the Lippert–Mataga equation[35] [Eq. (2)]:

$$\Delta\upsilon_{ST} = \frac{2\Delta\mu_{eg}^2}{hca_0^3}\left[\frac{\varepsilon-1}{2\varepsilon+1} - \frac{n^2-1}{2n^2+1}\right] + Const. \quad (2)$$

Within this dielectric continuum model, ε is the relative permittivity and n the refractive index of the solvent, h is the Planck constant and c is the speed of light. The Onsager radius, a_0, defined as the solvent shell around the molecule was estimated at a value of approximately 5.5 Å for both molecules. This value corresponds to 40% of the longest axis of the compound **3** as suggested by Lippert for nonspherical molecules.[35a] It should be emphasized that, for chromophore **5**, we assume that the relaxed S_1 state is not fully delocalized within the entire two-branched structure but is mainly localized on a single branch of the molecule. Such an assumption has been theoretically predicted for the relaxed S_1 state of multibranched chromophores with quadrupolar V-shaped geometries[14d] or octupolar trigonal symmetries.[36] Even though the solvatochromic measurements are performed over a limited range of the solvent polarity scale, the dipole moment change ($\Delta\mu_{ge}$) can be estimated to 15 ± 1 D and 19 ± 2 D for chromophores **3** and **5**, respectively. Such values are of the same magnitude as those obtained for "push-pull" trans-stilbenes such as 4-cyano-4′-dimethylaminostilbene[37] (~15 D) or 4-methoxy-4′-nitrostilbenes[4f,38] (~23 D) and therefore illustrate the significant charge transfer character of the emitting states.

The very low fluorescence quantum yield measured for **3** and **5** is a clear indication of the occurrence of very efficient nonradiative deactivation processes at the singlet excited state. We assume that the main relaxation process responsible for the fluorescence quenching of **3** and **5** corresponds to a conformational change of the excited state.

Trans-to-*cis* photoisomerization should be first excluded as a major nonradiative channel. Indeed, the measured quantum yield for this photoreaction ($\Phi_{t\rightarrow c}$) has a very low value (below 10^{-3}) both in hexane and dimethylformamide (N_2-degassed solutions). Such a weakly efficient photoisomerization presumably owes to a large activation barrier between the S_1 state and the double-bond-twisted excited species ^{1}P.[39] This so-called "phantom" ^{1}P state acts as a photochemical funnel (possibly through conical intersection) toward the ground state surface from which an equally probable isomerization to *cis* and *trans* occurs.[40] We can also exclude that a parallel photoisomerization reaction may occur by intersystem crossing (ISC).[41] In this case, the planar triplet state would undergo a barrierless C=C torsion to the ^{3}P state. However, one would expect that $\Phi_{t\rightarrow c}$ should be at least equal to half the value of Φ_{ISC} even though we assume that the triplet state mechanism constitutes the major photoisomerization pathway. Owing to the very low quantum yield measured for the photoisomerization ($<10^{-3}$), intersystem crossing should be considered as a negligible process with respect to the other deactivation pathways at the singlet excited state.

This assumption is also in line with the very weak phosphorescence measured for **3** and **5** in a glassy matrix of 2-methyl tetrahydrofuran (2 MTHF) (Figure S2). The phosphorescence spectrum, located in the $\lambda=600$–750 nm region is strongly overlapped with the fluorescence band. This suggests a relatively small energy difference between the S_1 and T_1 levels. As a consequence, a thermally activated delayed fluorescence emission is observed even at $T=77$ K. Moreover the delayed fluorescence lifetime is quite similar to that obtained for phosphorescence emission with values of approximately 15 μs. Notably, the very short lifetime measured for the phosphorescence of T_1 state is a clear indication of its $n\pi^*$ character. Hence, it appears that additional nonradiative processes at the S_1 state other than *trans*-to-*cis* photoisomerization and intersystem crossing should be taken into account to explain the weak fluorescence of the chromophores at room temperature.

Finally, we observed that high-viscosity solvents freeze down the molecular relaxation precesses in **3** and **5**. The temperature dependence of steady-state fluorescence spectra of **3** and **5** in 2MTHF is shown in Figure 7. The fluorescence quantum yields notably increase upon cooling the solutions. From $T=293$ K to 80 K Φ_f is multiplied by a factor of 430 and 105 for **3** and **5**, respectively. Two distinctive steps are clearly observed and both

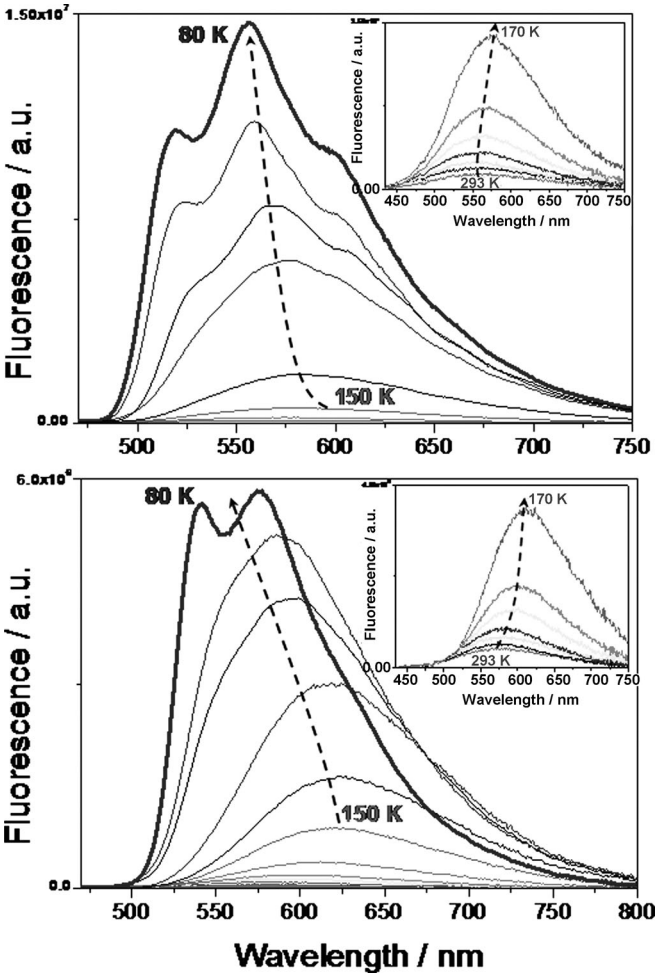

Figure 7. Fluorescence spectra of **3** and **5** in 2MTHF over the temperature range of 80-293 K.

dyes behave similarly in a qualitative sense. Decreasing the temperature from 293 K to 140 K results in a fluorescence enhancement of approximately eight times, and a gradual band redshift with a thermochromic slope of approximately 11 $cm^{-1}K^{-1}$ for **3** and approximately 14 $cm^{-1}K^{-1}$ for **5**. Upon further cooling, the bathochromic effects level off and below $T=130$ K the fluorescence bands reversely shift to the high-energy region with a sizeable increase in intensity.

It is well established that the dielectric constant and viscosity are two main physical properties of the surrounding medium that affect the fluorescence properties of chromophores.[42] In reference to 2MTHF, the relative influence of these two parameters evolves sequentially depending on the temperature range.[43] In the high-temperature region (i.e. above the glass-transition temperature, $T_g \approx 130$ K), the thermochromic shift should be mainly attributed to an increase in the effective solvent polarity owing to a continuous growth in the dielectric constant from 7 at $T=293$ K to a maximum value of 18 at $T=140$ K.[44] During the glass-transition step, the dielectric constant drops abruptly to 2.6 and remains quite constant from $T=110$ K to 77 K. Meanwhile, the viscosity increases exponentially from 10^2 $Pa\,s^{-1}$ to 3.5×10^{19} $Pa\,s^{-1}$. In this low temperature region, all conformational changes are severely restricted. This change in the solvent viscosity is clearly responsible for the dramatic fluorescence enhancement for **3** and **5** that is associated with band hypsochromy. As a consequence, we propose that the main relaxation process responsible for the fluorescence quenching of **3** and **5** corresponds to a conformational change from a nearly planar locally excited (^{1}LE) state to a twisted geometry; presumably a twisted intramolecular charge transfer (^{1}TICT) state.[45] This D/A decoupled geometry is expected to exhibit a forbidden optical transition that leads to a non-emissive (or weakly emissive) excited state (Scheme 4).

In reference to donor–acceptor-substituted stilbenes, two scenarios can be investigated. They all rely on the molecular structure of the stilbene, the nature of the D/A couples and the determination of the single bond involved in the torsional motion. Interestingly both twisting mechanisms strongly compete with the formation of the ^{1}P state, which is consistent with the very low *trans*-to-*cis* quantum yields observed for **3** and **5**. A first mechanism was proposed by Lapouyade et al. that is based on ring-bridged model stilbene derivatives.[37bc,46] In this mechanism, the formation of the ^{1}TICT state results in a rotation about a single bond adjacent to the central ethylene one. This hypothesis was proposed for *trans*-4-(*N*,*N*-dimethylamino)stilbenes or *trans*-4-(alkoxy)stilbenes with strong terminal acceptor groups (e.g. –CN, $–NO_2$) in the 4′ position. Such a precursor–successor mechanism affects the central part of the chromophore. In our case, this relaxation mode would induce a very large amplitude motion if the crowded V-shaped structure of **5** is considered. Therefore, one would expect to observe a significant activation barrier (E_a) between ^{1}LE and ^{1}TICT states (see Scheme 4). Interestingly, these latter activation barriers can be determined for **3** and **5**. Indeed, the nonradiative rate constant (k_{nr}) can be derived from the following relationship [Eq. (3)]:

$$\frac{k_{nr}}{k_r} = \frac{k_{IC} + k_{ISC} + k_a}{k_r} = \frac{1-\Phi_f}{\Phi_f} \qquad (3)$$

In this equation, the radiative rate constant of the emitting state (k_r) is considered not to correlate with temperature and the internal conversion (IC) is normally an unactivated process.[47] If we assume that intersystem crossing can be neglected as compared to the ^{1}LE→^{1}TICT process (k_a) and internal conversion, then one can derive that $k_{nr} \approx k_{IC} + k_a$. The Arrhenius plots of $\ln(k_{nr}/k_r)$ versus 1/T are presented in Figure 8 and

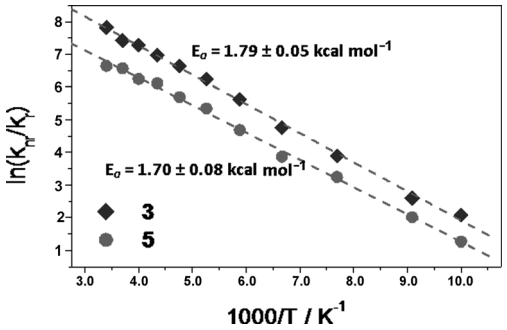

Figure 8. Arrhenius plot for the nonradiative-to-radiative rate constants ratio.

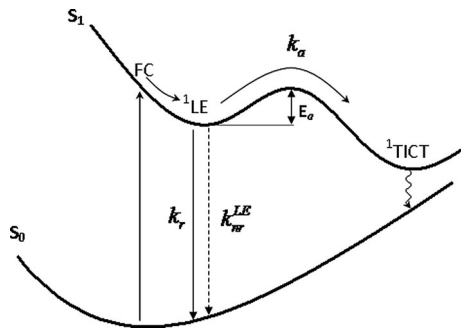

Scheme 4. Representation of the adiabatic TICT reaction pathway, in which S_0 and S_1 represent the ground and first electronic states, respectively. k_r = radiative rate constant, k_a = Arrhenius rate constant, k_{nr} = nonradiative rate constant, E_a = activation energy, LE = locally excited state, FC = Franck—Condon state, and TICT = twisted intramolecular charge transfer.

correlations are sufficiently linear to derive activation barriers in the 1.7–1.8 kcal mol^{-1} range. These values nicely coincide with the solvent viscosity barrier ($E_\eta \approx 1.82$ kcal mol^{-1} for 2MTHF)[48], which indicates that the ^{1}LE→^{1}TICT reaction does not proceed over a significant activation barrier and does not require a large-amplitude conformational change from the ^{1}LE state. Therefore this first mechanism is not reasonably transposable to our chromophores.

A second relaxation mechanism has been evidenced and extensively studied by Yang et al.[47a,49] This model was proposed for some aryl-substituted stilbenes such as N-aryl-substituted *trans*-4-aminostilbenes. Notably, the molecular structure of these derivatives is quite similar to that of our compounds.

The conformational change at the excited state results in a rotation about the single bond that connects the stilbenyl structure with the external aromatic subunit. This mechanism is more in line with the barrierless nature of the reaction because it only implies the relative motion of a peripherical part of the molecule with the rotation of a methylenepyran group from a twist angle of approximately 28° (see DFT calculation) to 90° with respect to the 4-styrylpyrimidine fragment (Scheme 1).

3. Conclusions

A linear and a V-shaped pyrimidine-based chromophore bearing γ-methylenepyrans as terminal donor groups have been synthesized. According to a large set of experimental data supported by DFT theoretical calculations, the photophysical properties of these new NLO organic materials have been methodically untangled. The branching effect is well described within the Frenkel exciton model and leads to a moderate interbranch coupling. The ground state structure of both derivatives shows a significant twisting of the pyranilydene groups with respect to the planar electron-deficient pyrimidine core. Such a deviation from planarity of the chromophores does not allow an optimal electronic conjugation all along the molecular scaffold. As a consequence, the NLO response is modest relative to that of other π-conjugated derivatives with similar size and architecture. In the same manner, the rotation of the donor end-group has a decisive influence on the excited-state dynamics, which leads to a detrimental fluorescence quenching effect. Therefore, we demonstrate here that the flexibility of a simple structural parameter both affects the NLO properties as well as the dyes emissivity. Preventing this specific rotation would presumably lead to a synergetic effect. A ring-bridged strategy is currently underway.

Experimental Section

Materials and general methods: In air and moisture-sensitive reactions, all glassware was flame-dried and cooled under nitrogen. All other commercially available reactants were used without further purification. The solvents used for absorption and emission analysis were as follows: ethyl acetate (ETA), 2-methyl tetrahydrofuran (2MTHF), tetrahydrofuran (THF), dichloromethane (CH_2Cl_2), acetone (ACT), dimethylformamide (DMF). All the solvents employed were Aldrich, Fluka or Merck spectroscopic grade. Compounds **1** and **4** were prepared as previously described.[21b] NMR spectra were acquired at RT on a Bruker DRX500 spectrometer at the Service Commun de Recherche de Résonance Magnétique Nucléaire et de Résonance Paramagnétique Electronique de l'Université de Bretagne Occidentale. Chemical shifts are given in parts per million relative to TMS (1H, $\delta = 0.0$ ppm) and $CDCl_3$ (13C, $\delta = 77.0$ ppm). Acidic impurities in $CDCl_3$ were removed by treatment with anhydrous K_2CO_3. High resolution mass analyses were performed at the Centre Régional de Mesures Physiques de l'Ouest (CRMPO, University of Rennes1) by using a Bruker MicroTOF-Q II apparatus.

General procedure for the Wittig reaction: A small excess of *n*-butyllithium (1.1 equiv; 2.5 M in hexanes) was added dropwise at $T = -78$ °C, under a nitrogen atmosphere, to a degassed solution of 2,6-diphenyl-4*H*-pyran-4-yl triphenylphosphonium tetrafluoroborate salt **2**[21] (1 equiv) in dry THF. After 15 min, the carboxaldehyde (0.9 equiv and 0.45 in the case of compound **4**) was added. The solution was stirred at $T = -78$ °C for 30 min, and allowed to warm to RT for 2 h. The THF was evaporated and the residue was dissolved in a 1:1 mixture of CH_2Cl_2/water (100 mL) and the organic layer was separated. The aqueous layer was extracted with CH_2Cl_2 (2× 50 mL). The combined organic extracts were dried with $MgSO_4$ and the solvents evaporated.

(E)4-{2-[4-(2,6-Diphenyl-pyran-4-ylidenemethyl)-phenyl]-vinyl}-pyrimidine (**3**): Red solid; obtained according to general procedure and purified by column chromatography (SiO_2, CH_2Cl_2/ETA, 1:1) followed by crystallization from $CHCl_3$/n-heptane; yield 65% (277 mg); mp: 227–228 °C (decomposes); ^{1}H NMR (500 MHz, $CDCl_3$): $\delta = 5.94$ (s, 1H), 6.44 (s, 1H), 7.04 (s, 1H), 7.05 (d, 1H, $J = 16$ Hz), 7.31 (d, 1H, $J = 5$ Hz), 7.42–7.46 (m, 8H), 7.59 (d, 2H, $J = 8$ Hz), 7.76–7.78 (m, 4H), 7.89 (d, 1H, $J = 16$ Hz), 7.66 (d, 1H, $J = 5$ Hz), 9.16 ppm (s, 1H); ^{13}C NMR and JMOD (125 MHz, $CDCl_3$): $\delta =$ 162.5 (C), 158.9 (CH), 157.3 (CH), 153.3 (C), 151.3 (C), 140.3 (C), 137.3 (CH), 133.4 (C), 133.2 (C), 132.6 (C), 130.5 (C), 129.5 (CH), 129.2 (CH), 128.8 (CH), 128.70 (CH), 128.70 (CH), 128.1 (CH), 125.0 (CH), 124.6 (CH), 124.3 (CH), 118.6 (CH), 113.7 (CH), 108.7 (CH), 102.2 ppm (CH). HRMS (ESI/ASAP) *m/z*: calcd for $C_{30}H_{23}N_2O$ $[M+H]^+$: 427.1810; found: 427.1804.

4,6-Bis-{2-[4-(2,6-diphenyl-pyran-4-ylidenemethyl)-phenyl]-vinyl}-pyrimidine (**5**): Red solid; obtained according to general procedure and purified by column chromatography (SiO_2, CH_2Cl_2/ETA, 7:3) followed by crystallization from $CHCl_3$/*n*-heptane; yield 31% (240 mg); mp: 243–244 °C (decomposes); ^{1}H NMR (500 MHz, $CDCl_3$): $\delta = 5.95$ (s, 2H), 6.45 (s, 2H), 7.06 (s, 2H), 7.08 (d, 2H, $J = 16$ Hz), 7.28 (s, 1H), 7.40–7.48 (m, 16H), 7.61 (d, 4H, $J = 8$ Hz), 7.77–7.79 (m, 8H), 7.92 (d, 2H, $J = 16$ Hz), 9.10 ppm (s, 1H); ^{13}C NMR and JMOD (125 MHz, $CDCl_3$): $\delta = 162.9$ (C), 158.7 (CH), 153.2 (C), 151.2 (C), 140.1 (C), 136.8 (CH), 133.4 (C), 133.2 (C), 132.8 (C), 130.5 (C), 129.5 (CH), 129.2 (CH), 128.71 (CH), 128.69 (CH), 128.1 (CH), 128.0 (CH), 125.0 (CH), 124.7 (CH), 124.6 (CH), 116.4 (CH), 113.8 (CH), 108.8 (CH), 102.2 ppm (CH). HRMS (ESI): *m/z*: calcd for $C_{56}H_{41}N_2O_2$ $[M+H]^+$: 773.3168; found: 773.3163.

Steady-state absorption and fluorescence spectra: The absorption measurements were performed with a PerkinElmer Lambda 2 spectrometer. Steady-state fluorescence and phosphorescence spectra were collected from a FluoroMax-4 spectrofluorometer. Emission spectra were spectrally corrected, and fluorescence quantum yields include the correction owing to solvent refractive index and were determined relative to quinine bisulfate in sulfuric acid (0.05M, $\Phi_{ref} = 0.52$)[50] Owing to the very weak emissive chromophores ($\Phi_f < 10^{-3}$), the fluorescence quantum yields were obtained from 5 independent measurements and the uncertainties were determined to ±20%. Phosphorescence and steady-state anisotropy measurements were performed in 2-methyl tetrahydrofuran at $T =$ 77 K. The samples were placed in a 5 mm diameter quartz tube inside a Dewar flask filled with liquid nitrogen.

Time-gated luminescence: The phosphorescence lifetimes were measured by using a FluoroMax-4 spectrofluorometer that was also equipped with a Xe-pulsed lamp operating at up to $f = 25$ Hz. The phosphorescence decays were obtained according to a time-gated method. The emission was recorded by using a control module that included a gate-and-delay generator, which allowed the integration of the signal during a specific period after a flash (delay) and for a pre-determined time window. The total signal was accumulated for a large number of excited pulses.

Fluorescence anisotropy: For the steady-state anisotropy measurements, two Glan-Thompson polarizers were placed in the excita-

tion and emission beams. The anisotropy r is determined as follows in Equation (4):

$$r = \frac{I_{VV} - gI_{VH}}{I_{VV} + 2.g.I_{VH}} g = \frac{I_{HV}}{I_{HH}} \quad (4)$$

in which I is the fluorescence intensity. The subscripts denote the orientation (horizontal H or vertical V) of the excitation and emission polarizers, respectively. g is an instrumental correction factor. The proper calibration of the set-up was checked by using a recent standard method with rhodamine 101 in glycerol.[51]

Low-temperature measurements: Low-temperature emission measurements were performed in 2MTHF by using an Oxford Cryogenics OptistatDN cryostat fitted with an Oxford Instruments ITC503S temperature controller. The temperature dependency of the refractive index and the density of the solvent were taken into account for the measurement of Φ_f.[52]

Cyclic voltammetry: The cyclic voltammetry experiments[53] (conducted by using a computer-controlled Radiometer Voltalab 6 potentiostat with a three-electrode single compartment cell; the working electrode was a platinum disk; a saturated calomel electrode (SCE) used as a reference was placed in a separate compartment with a salt bridge containing the supporting electrolyte) were performed at $T = 300$ K, in N_2-degassed dichloromethane with a constant concentration (0.1 M) of nBu$_4$BF$_4$. Ferrocene (Fc) was used as an internal reference (considering $E_{Fc/Fc+} = 0.53$ V in CH_2Cl_2 vs the aqueous SCE).[54]

Actinometry: quantum yields for *trans*→*cis* photoisomerization were measured under irradiation at $\lambda = 436$ nm by using a 100 W Mercury-Xenon Lamp (Hamamatsu, L2422-02) equipped with a band pass filter (THORLAB, FB430-10). All irradiated solutions were previously N_2-degassed. The progress of the photoreaction was monitored by UV/Vis absorption spectra. The absorbance at the excitation wavelength had to be greater than 2 to assume a total absorption of the incident photons. The incident light intensity was measured by ferrioxalate actinometry.[55]

Open-aperture Z-scan method: The two-photon absorption spectra were measured by using the open-aperture Z-scan method[30] with a femtosecond mode-locked Ti: Sapphire laser (Coherent, Chameleon Ultra II: pulse duration: 140 ± 20 fs; repetition rate: 80 MHz; wavelength range: 680–1080 nm). After passing through a beam expander (×4), the laser beam was focused by an $f = 15$ cm lens and passed through a quartz cell (1 mm optical path length). The position of the sample cell was varied along the laser-beam direction (z-axis) by using a Z-step motorized stage controlled by a computer. At constant incident excitation, the local power density within the sample was changed, and the corresponding transmitted laser beam, T(z), recorded with a silicon photodetector (Ophir PD300) was monitored in connection with the z-position of the cell. The on-axis peak intensity of the incident pulses at the focal point, I_0, ranged from 30 to 90 GW cm^{-2}. If we assume that the linear absorption of the sample is negligible at working wavelength and that the laser exhibits a Gaussian beam profile in space and time, the nonlinear absorption coefficient β can be calculated from the curve fitting to the experimental transmittance with the Equation (5):

$$T(z) = 1 - \frac{\beta I I_0}{2\sqrt{2}(1 + (\frac{z}{z_0})^2)} \quad (5)$$

in which z_0 is the coordinate along the propagation direction of the focal point of the beam, l the optical path length. The 2PA cross-section, δ, (in units of 1 GM: 10^{-50} cm^4 s^{-1} photon^{-1} molecule^{-1}) is then determined by using the relationship [Eq. (6)]:

$$\beta = \frac{\delta N_A d}{h\upsilon} 10^{-3} \quad (6)$$

in which h is the Planck constant, υ the frequency of the incident laser beam, N_A the Avogadro constant and d is the concentration of the chromophore (mol L^{-1}). The rhodamine 6G in methanol[56] (16.2 ± 2.4 GM at 806 nm) was used for the calibration of our measurement technique. The uncertainty in δ is of the order of 20%.

EFISHG measurements: The molecular quadratic optical nonlinearities of chromophores, in the form of $\mu g \beta$ products (μg is the ground state permanent dipole moment and β the first hyperpolarizability of the molecules, according to convention B),[57] were measured on a standard Electric Field Induced Second Harmonic Generation (EFISHG) set-up[58] operating at a $\lambda = 1907$ nm fundamental wavelength, obtained by Raman-shifting the emission from a Nd:YAG laser, which has the advantage of distance from the absorption bands of the molecules.

DFT calculations: The theoretical absorption spectra were computed based on Density Functional Theory (DFT) and Time-Dependent DFT (TDDFT). The overall computation strategy was defined as follows: after initial AM1 optimization calculations (vacuum), subsequent optimization of geometrical structures of the derivatives were performed using the PBE0/6-31G(d) level of calculation. (Notably, the PBE0 is a good functional for the description of photofunctional molecules).[59] Finally, the TDDFT vertical transitions were computed by using the same level of calculations. All calculations were performed by using the Gaussian 09 package.[60]

Keywords: chromophores · conjugation · heterocycles · nonlinear optics · photophysics

[1] S. Sumalekshmy, C. Fahrni, *J. Chem. Mater.* **2011**, *23*, 483 – 500.
[2] W. Denk, J. H. Strickler, W. Webb, *Science* **1990**, *248*, 73 – 76.
[3] a) K. J. McEwan, P. A. Fleitz, J. E. Rogers, J. E. Slagle, D. G. McLean, H. Akdas, M. Katterle, I. M. Blake, H. L. Anderson, *Adv. Mater.* **2004**, *16*, 1933 – 1935; b) Y. Morel, A. Irimia, P. Najechalski, Y. Kervella, O. Stephan, P. L. Baldeck, C. Andraud, *J. Chem. Phys.* **2001**, *114*, 5391 – 5396; c) J. E. Ehrlich, W. L. Wu, Y. L. Lee, Z. Y. Hu, H. Rockel, S. R. Marder, J. W. Perry, *Opt. Lett.* **1997**, *22*, 1843 – 1845.
[4] a) C. N. LaFratta, J. T. Fourkas, T. Baldacchini, R. A. Farrer, *Angew. Chem.* **2007**, *119*, 6352 – 6374; *Angew. Chem. Int. Ed.* **2007**, *46*, 6238 – 6258; b) S. Kawata, H.-B. Sun, T. Tanaka, K. Takada, *Nature* **2001**, *412*, 697 – 698; c) H.-B. Sun, S. Kawata, *Two-Photon Photopolymerization and 3D Lithographic Microfabrication, Vol. 170*, Springer, Berlin, **2004**; d) M. Jin, J. P. Malval, D. L. Versace, F. Morlet-Savary, H. Chaumeil, A. Defoin, X. Allonas, J. P. Fouassier, *Chem. Commun.* **2008**, 6540 – 6542; e) J. P. Malval, M. Jin, F. Morlet-Savary, H. Chaumeil, A. Defoin, O. Soppera, T. Scheul, M. Bouriau, P. L. Baldeck, *Chem. Mater.* **2011**, *23*, 3411 – 3420; f) J. P. Malval, F. Morlet-Savary, H. Chaumeil, L. Balan, D.-L. Versace, M. Jin, A. Defoin, *J. Phys. Chem. C* **2009**, *113*, 20812 – 20821; g) R. Xia, J. P. Malval, M. Jin, A. Spangenberg, D. Wan, H. Pu, T. Vergote, F. Morlet-Savary, H. Chaumeil, P. Baldeck, O. Poizat, O. Soppera, *Chem. Mater.* **2012**, *24*, 237 – 244.
[5] a) W. H. Zhou, S. M. Kuebler, K. L. Braun, T. Y. Yu, J. K. Cammack, C. K. Ober, J. W. Perry, S. R. Marder, *Science* **2002**, *296*, 1106 – 1109; b) B. H. Cumpston, S. P. Ananthavel, S. Barlow, D. L. Dyer, J. E. Ehrlich, L. L. Erskine, A. A.; Heika, S. M. Kuebler, I.-Y. S. M.; Lee, D. McCord-Maughon, J. Qin, H. Röckel, M. Rumi, X.-L. Wu, S. R. Marder, J. W. Perry, *Nature* **1999**, *398*, 51 – 54.

[6] a) G. S. He, L.-S. Tan, Q. Zheng, P. N. Prasad, *Chem. Rev.* **2008**, *108*, 1245 – 1330; b) M. Pawlicki, H. A. Collins, R. G. Denning, H. L. Anderson, *Angew. Chem.* **2009**, *121*, 3292 – 3316; *Angew. Chem. Int. Ed.* **2009**, *48*, 3244 – 3266.
[7] A. Bhaskar, G. Ramakrishna, Z. Lu, R. Twieg, J. M. Hales, D. J. Hagan, E. V. Stryland, T. Goodson, *J. Am. Chem. Soc.* **2006**, *128*, 11840 – 11849.
[8] a) M. G. Kuzyk, *J. Chem. Phys.* **2003**, *119*, 8327 – 8334; b) J. Pérez-Moreno, M. G. Kuzyk, *J. Chem. Phys.* **2005**, *123*, 194101.
[9] a) M. Johnsen, M. J. Paterson, J. Arnbjerg, O. Christiansen, C. B. Nielsen, M. Jorgensen, P. R. Ogilby, *Phys. Chem. Chem. Phys.* **2008**, *10*, 1177 – 1191; b) M. Rumi, J. E. Ehrlich, A. Heikal, J. W. Perry, S. Barlow, Z. Y. Hu, D. McCord-Maughon, T. C. Parker, H. Rockel, S. Thayumanavan, S. R. Marder, D. Beljonne, J. L. Brédas, *J. Am. Chem. Soc.* **2000**, *122*, 9500 – 9510.
[10] a) K. D. Belfield, M. V. Bondar, F. E. Hernandez, O. V. Przhonska, S. Yao, *J. Phys. Chem. B* **2007**, *111*, 12723 – 12729; b) K. D. Belfield, A. R. Morales, B.-S. Kang, J. M. Hales, D. J. Hagan, E. W. V. Stryland, V. M. Chapela, J. Percino, *Chem. Mater.* **2004**, *16*, 4634 – 4641; c) K. D. Belfield, K. J. Schafer, W. Mourad, B. A. Reinhardt, *J. Org. Chem.* **2000**, *65*, 4475 – 4481.
[11] O. K. Kim, K. S. Lee, Z. Huang, W. B. Heuer, C. S. Paik-Sung, *Opt. Mater.* **2003**, *21*, 559 – 564.
[12] a) T. K. Ahn, K. S. Kim, D. Y. Kim, S. B. Noh, N. Aratani, C. Ikeda, A. Osuka, D. Kim, *J. Am. Chem. Soc.* **2006**, *128*, 1700 – 1704; b) M.-C. Yoon, S. B. Noh, A. Tsuda, Y. Nakamura, A. Osuka, D. Kim, *J. Am. Chem. Soc.* **2007**, *129*, 10080 – 10081; c) S. Drouet, A. Merhi, D. D. Yao, M. P. Cifuentes, M. G. Humphrey, M. Wielgus, J. Olesiak-Banska, K. Matczyszyn, M. Samoc, F. Paul, C. O. Paul-Roth, *Tetrahedron* **2012**, *68*, 10351 – 10359.
[13] a) D. Beljonne, W. Wenseleers, E. Zojer, Z. Shuai, H. Vogel, S. J. K. Pond, J. W. Perry, S. R. Marder, J. L. Brédas, *Adv. Funct. Mater.* **2002**, *12*, 631 – 641; b) C. K. M. Chan, C. H. Tao, K.-F. Li, K. M. C. Wong, N. Y. Zhu, K.-W. Cheah, V. W.-W. Yam, *Dalton Trans.* **2011**, *40*, 10670 – 10685.
[14] a) S. J. K. Pond, O. Tsutsumi, M. Rumi, O. Kwon, E. Zojer, J. L. Brédas, S. R. Marder, J. W. Perry, *J. Am. Chem. Soc.* **2004**, *126*, 9291 – 9306; b) S. J. Chung, M. Rumi, V. Alain, S. Barlow, J. W. Perry, S. R. Marder, *J. Am. Chem. Soc.* **2005**, *127*, 10844 – 10845; c) C. Katan, S. Tretiak, M. H. V. Werts, A. J. Bain, R. J. Marsh, N. Leonczek, N. Nicolaou, E. Badaeva, O. Mongin, M. Blanchard-Desce, *J. Phys. Chem. B* **2007**, *111*, 9468 – 9483; d) C. Katan, F. Terenziani, O. Mongin, M. H. V. Werts, L. Porrès, T. Pons, J. Mertz, S. Tretiak, M. Blanchard-Desce, *J. Phys. Chem. A* **2005**, *109*, 3024 – 3037.
[15] a) C. Katan, S. Tretiak, J. Even, *Proc. SPIE* **2010**, *7712*, 77123D; b) H. Akdas-Kilig, J. P. Malval, F. Morlet-Savary, A. Singh, L. Toupet, I. Ledoux-Rak, J. Zyss, H. Le Bozec, *Dyes Pigm.* **2012**, *92*, 681 – 688.
[16] a) A. Adronov, J. M. J. Fréchet, G. S. He, K.-S. Kim, S.-J. Chung, J. Swiatkiewicz, P. N. Prasad, *Chem. Mater.* **2000**, *12*, 2838 – 2841; b) M. Drobizhev, A. Karotki, Y. Dzenis, A. Rebane, Z. Suo, C. W. Spangler, *J. Phys. Chem. B* **2003**, *107*, 7540 – 7543; c) A. Abbotto, L. Beverina, R. Bozio, A. Facchetti, C. Ferrante, G. A. Pagani, D. Pedron, R. Signorini, *Chem. Commun.* **2003**, 2144 – 2145; d) K. A. Green, M. P. Cifuentes, M. Samoc, M. G. Humphrey, *Coord. Chem. Rev.* **2011**, *255*, 2025 – 2038.
[17] a) S. Achelle, N. Plé, *Curr. Org. Synth.* **2012**, *9*, 163 – 187; b) S. Achelle, A. Barsella, C. Baudequin, B. Caro, F. Robin-le Guen, *J. Org. Chem.* **2012**, *77*, 4087 – 4096; c) S. Achelle, N. Saettel, P. Baldeck, M. P. Teulade-Fichou, P. Maillard, *J. Porphyrins Phthalocyanines* **2010**, *14*, 877 – 884.
[18] a) N. Faux, F. Robin-le Guen, P. le Poul, B. Caro, K. Nakatani, E. Ishow, S. Golhen, *Eur. J. Inorg. Chem.* **2006**, 3489 – 3497; b) R. Andreu, L. Carrasquer, S. Franco, J. Garin, J. Orduna, N. M. de Baroja, R. Alicante, B. Villacampa, M. Allain, *J. Org. Chem.* **2009**, *74*, 6647 – 6657; c) R. Andreu, E. Galan, J. Garin, V. Herrero, E. Lacarra, J. Orduna, R. Alicante, B. Villacampa, *J. Org. Chem.* **2010**, *75*, 1684 – 1692; d) R. Andreu, E. Galán, J. Orduna, B. Villacampa, R. Alicante, J. T. L. Navarrete, J. Casado, J. Garín, *Chem. Eur. J.* **2011**, *17*, 826 – 838.
[19] a) S. R. Marder, D. N. Beratan, L.-T. Cheng, *Science* **1991**, *252*, 103 – 106; b) G. Bourhill, J. L. Bredas, L.-T. Cheng, S. R. Marder, F. Meyers, J. W. Perry, B. G. Tiemann, *J. Am. Chem. Soc.* **1994**, *116*, 2619 – 2620; c) I. D. L. Albert, T. J. Marks, M. A. Ratner, *J. Am. Chem. Soc.* **1997**, *119*, 3155 – 3156.
[20] a) J.-J. Vanden Eynde, L. Pascal, Y. Van Haverbeke, P. Dubois, *Synth. Commun.* **2001**, *31*, 3167 – 3173; b) L. Pascal, J. J. V. Eynde, Y. Van Haverbeke, P. Dubois, A. Michel, U. Rant, E. Zojer, G. Leising, L. O. Van Dorn, N. E. Gruhn, J. Cornil, J. L. Brédas, *J. Phys. Chem. B* **2002**, *106*, 6442 – 6450.
[21] C. H. Chen, G. A. Reynolds, *J. Org. Chem.* **1980**, *45*, 2453 – 2458.
[22] F. Ba, F. Robin-Le Guen, N. Cabon, P. Le Poul, S. Golhen, N. Le Poul, B. Caro, *J. Organomet. Chem.* **2010**, *695*, 235 – 243.
[23] J. R. Platt, *J. Chem. Phys.* **1949**, *17*, 484 – 495.
[24] F. Ba, N. Cabon, F. Robin-Le Guen, P. Le Poul, N. Le Poul, Y. Le Mest, S. Golhen, B. Caro, *Organometallics* **2008**, *27*, 6396 – 6399.
[25] F. Ba, N. Cabon, P. le Poul, S. Kahlal, J.-Y. Saillard, N. le Poul, S. Golhen, B. Caro, F. Robin-le Guen, *New J. Chem.* **2013**, DOI: 10.1039/C3NJ41126E.
[26] K. Itami, D. Yamazaki, J. Yoshida, *J. Am. Chem. Soc.* **2004**, *126*, 15396 – 15397.
[27] S. Dufresne, G. S. Hanan, W. G. Skene, *J. Phys. Chem. B* **2007**, *111*, 11407 – 11418.
[28] A. S. Davidov, *Theory of Molecular Excitons*, Plenum, New York, **1971**.
[29] F. Terenziani, C. Katan, E. Badaeva, S. Tretiak, M. Blanchard-Desce, *Adv. Mater.* **2008**, *20*, 4641 – 4678.
[30] a) M. Sheik-Bahae, A. A. Said, E. W. V. Stryland, *Opt. Lett.* **1989**, *14*, 955 – 957; b) M. Sheik-Bahae, A. A. Said, T. H. Wei, D. J. Hagan, E. W. V. Stryland, *IEEE J. Quantum Electron.* **1990**, *26*, 760 – 769.
[31] a) J. P. Malval, J. P. Morand, R. Lapouyade, W. Rettig, G. Jonusauskas, J. Oberle, C. Trieflinger, J. Daub, *Photochem. Photobiol. Sci.* **2004**, *3*, 939 – 948; b) D. Rehm, A. Weller, *Isr. J. Chem.* **1970**, *8*, 259.
[32] L. Antonov, K. Kamada, K. Ohta, F. S. Kamounah, *Phys. Chem. Chem. Phys.* **2003**, *5*, 1193 – 1197.
[33] Y.-Z. Cui, Q. Fang, G. Xue, G.-B. Xu, L. Yin, W.-T. Yu, *Chem. Lett.* **2005**, *34*, 644 – 645.
[34] a) K. D. Singer, A. F. Garito, *J. Phys. Chem.* **1981**, *75*, 3572 – 3580; b) B. F. Levine, C. G. Bethea, *Appl. Phys. Lett.* **1974**, *24*, 445 – 447; c) I. Ledoux, J. Zyss, *Chem. Phys.* **1982**, *73*, 203 – 213.
[35] a) E. Z. Lippert, *Z. Naturforsch. A* **1955**, *10a*, 541 – 545; b) N. Mataga, Y. Kaifu, M. Koizumi, *Bull. Chem. Soc. Jpn.* **1955**, *28*, 690 – 691.
[36] a) W. Verbouwe, M. Van der Auweraer, F. C. De Schryver, J. J. Piet, J. M. Warman, *J. Am. Chem. Soc.* **1998**, *120*, 1319 – 1324; b) W. Verbouwe, L. Viaene, M. Van der Auweraer, F. C. De Schryver, H. Masuhara, R. Pansu, J. Faure, *J. Phys. Chem. A* **1997**, *101*, 8157 – 8165.
[37] a) N. P. Ernsting, J. Breffke, D. Y. Vorobyev, D. A. Duncan, I. Pfeffer, *Phys. Chem. Chem. Phys.* **2008**, *10*, 2043 – 2049; b) J. F. Letard, R. Lapouyade, W. Rettig, *J. Am. Chem. Soc.* **1993**, *115*, 2441 – 2447; c) R. Lapouyade, K. Czeschka, W. Majenz, W. Rettig, E. Gilabert, C. Rulliere, *J. Phys. Chem.* **1992**, *96*, 9643 – 9650; d) Y. V. Il'ichev, W. Kuhnle, K. A. Zachariasse, *Chem. Phys.* **1996**, *211*, 441 – 453.
[38] H. Gruen, H. Görner, *J. Phys. Chem.* **1989**, *93*, 7144 – 7152.
[39] a) D. H. Waldeck, *Chem. Rev.* **1991**, *91*, 415 – 436; b) J. Saltiel, A. S. Waller, D. F. Sears, E. A. Hoburg, D. M. Zeglinski, D. H. Waldeck, *J. Phys. Chem.* **1994**, *98*, 10689 – 10698.
[40] a) H. Görner, *J. Photochem. Photobiol. A* **1987**, *40*, 325 – 339; b) H. Görner, D. Schulte-Frohlinde, *J. Photochem.* **1978**, *8*, 91 – 102; c) V. Papper, D. Pines, G. Likhtenshtein, E. Pines, *J. Photochem. Photobiol. A* **1997**, *111*, 87 – 96.
[41] a) J. Saltiel, A. Marinari, D. W. L. Chang, J. C. Mitchener, E. D. Megarity, *J. Am. Chem. Soc.* **1979**, *101*, 2982 – 2996; b) H. Görner, D. Schulte-Frohlinde, *J. Phys. Chem.* **1978**, *82*, 2653 – 2659.
[42] a) P. J. Suppan, *Photochem. Photobiol. A* **1990**, *50*, 293 – 330; b) T. Hagan, D. Pilloud, P. Suppan, *Chem. Phys. Lett.* **1987**, *139*, 499 – 502.
[43] a) T. Furutsuka, T. Imura, T. Kojima, K. Kawabe, *Technol. Rep. Osaka Univ.* **1974**, 367; b) A. C. Ling, J. E. Willard, *J. Phys. Chem.* **1968**, *72*, 1918 – 1923.
[44] a) G. U. Bublitz, S. G. Boxer, *J. Am. Chem. Soc.* **1998**, *120*, 3988 – 3992; b) M. Goes, M. de Groot, M. Koeberg, J. W. Verhoeven, N. R. Lokan, M. J. Shephard, M. N. Paddon-Row, *J. Phys. Chem. A* **2002**, *106*, 2129 – 2134.
[45] Z. R. Grabowski, K. Rotkiewicz, W. Rettig, *Chem. Rev.* **2003**, *103*, 3899 – 4032.
[46] a) H. El-Gezawy, W. Rettig, R. Lapouyade, *J. Phys. Chem. A* **2006**, *110*, 67 – 75; b) R. Lapouyade, A. Kuhn, J. F. Letard, W. Rettig, *Chem. Phys. Lett.* **1993**, *208*, 48 – 58; c) W. Rettig, W. Majenz, R. Herter, J.-F. Létard, R. Lapouyade, *Pure Appl. Chem.* **1993**, *65*, 1699 – 1704; d) E. Abraham, J. Oberlé, G. Jonusauskas, R. Lapouyade, C. Rullière, *J. Photochem. Photobiol. A* **1997**, *105*, 101 – 107; e) J.-F. Letard, R. Lapouyade, W. Rettig, *Chem. Phys.* **1994**, *186*, 119 – 131; f) E. Abraham, J. Oberlé, G. Jonusauskas, R. Lapouyade, C. Rullière, *Chem. Phys.* **1997**, *214*, 409 – 423.
[47] a) J.-S. Yang, K.-L. Liau, C.-M. Wang, C.-Y. Hwang, *J. Am. Chem. Soc.* **2004**, *126*, 12325 – 12335; b) F. D. Lewis, W. Weigel, *J. Phys. Chem. A* **2000**, *104*,

8146 – 8153; c) F. D. Lewis, W. Weigel, X. Zuo, *J. Phys. Chem. A* **2001**, *105*, 4691 – 4696; d) F. D. Lewis, R. S. Kalgutkar, J.-S. Yang, *J. Am. Chem. Soc.* **1999**, *121*, 12045 – 12053.
[48] C.-C. Cheng, W.-S. Yu, P.-T. Chou, S.-M. Peng, G.-H. Lee, P.-C. Wu, Y.-H. Song, Y. Chi, *Chem. Commun.* **2003**, 2628 – 2629.
[49] a) J.-S. Yang, S.-Y. Chiou, K.-L. Liau, *J. Am. Chem. Soc.* **2002**, *124*, 2518 – 2527; b) J.-Y. Yang, K.-L. Liau, C.-Y. Hwang, C.-M. Wang, *J. Phys. Chem. A* **2006**, *110*, 8003 – 8010; c) J.-Y. Yang, C.-K. Lin, A. M. Lahoti, C.-K. Tseng, Y.-H. Liu, G.-H. Lee, S.-M. Peng, *J. Phys. Chem. A* **2009**, *113*, 4868 – 4877; d) J.-S. Yang, K.-L. Liau, C.-Y. Li, M.-Y. Chen, *J. Am. Chem. Soc.* **2007**, *129*, 13183 – 13192.
[50] R. Meech, D. Phillips, *J. Photochem.* **1983**, *23*, 193 – 217.
[51] T. J. V. Prazeres, A. Fedorov, S. P. Barbosa, J. M. G. Martinho, M. N. Berberan-Santos, *J. Phys. Chem. A* **2008**, *112*, 5034 – 5039.
[52] T. Rong-Ri, S. Xin, H. Lin, Z. Feng-Shou, *Chin. Phys. B* **2012**, *21*, 086402.
[53] J.-P. Malval, C. Chaimbault, B. Fischer, J.-P. Morand, R. Lapouyade, *Res. Chem. Intermed.* **2001**, *27*, 21 – 34.
[54] P. Hapiot, L. D. Kispert, V. V. Konovalov, J.-M. Savéant, *J. Am. Chem. Soc.* **2001**, *123*, 6669 – 6677.
[55] M. Montalti, A. Credi, L. Prodi, M. T. Gandolfi, *Handbook of Photochemistry, 3rd ed.*, CRC, Boca Raton, **2006**.
[56] P. Sengupta, J. Balaji, S. Banerjee, R. Philip, G. R. Kumar, S. Maiti, *J. Chem. Phys.* **2000**, *112*, 9201 – 9205.
[57] a) A. Willetts, J. E. Rice, D. M. Burland, *J. Chem. Phys.* **1992**, *97*, 7590 – 7599; Burland, *J. Chem. Phys.* **1992**, *97*, 7590 – 7599; b) H. Reis, *J. Chem. Phys.* **2006**, *125*, 014506.
[58] T. Thami, P. Bassoul, M. A. Petit, J. Simon, A. Fort, M. Barzoukas, A. Villayes, *J. Am. Chem. Soc.* **1992**, *114*, 915 – 921.
[59] S. Aloïse, Z. Pawlowska, C. Ruckebusch, M. Sliwa, J. Dubois, O. Poizat, G. Buntinx, A. Perrier, F. Maurel, P. Jacques, J.-P. Malval, L. Poisson, G. Piani, J. Abe, *Phys. Chem. Chem. Phys.* **2012**, *14*, 1945 – 1956.
[60] Gaussian 09 (Revision B.01), M. J. Frisch, G. W. Trucks, H. B. Schlegel, G. E. Scuseria, M. A. Robb, J. R. Cheeseman, G. Scalmani, V. Barone, B. Mennucci, G. A. Petersson, H. Nakatsuji, M. Caricato, X. Li, H. P. Hratchian, A. F. Izmaylov, J. Bloino, G. Zheng, J. L. Sonnenberg, M. Hada, M. Ehara, K. Toyota, R. Fukuda, J. Hasegawa, M. Ishida, T. Nakajima, Y. Honda, O. Kitao, H. Nakai, T. Vreven, J. A. Montgomery, Jr., J. E. Peralta, F. Ogliaro, M. Bearpark, J. J. Heyd, E. Brothers, K. N. Kudin, V. N. Staroverov, R. Kobayashi, J. Normand, K. Raghavachari, A. Rendell, J. C. Burant, S. S. Iyengar, J. Tomasi, M. Cossi, N. Rega, J. M. Millam, M. Klene, J. E. Knox, J. B. Cross, V. Bakken, C. Adamo, J. Jaramillo, R. Gomperts, R. E. Stratmann, O. Yazyev, A. J. Austin, R. Cammi, C. Pomelli, J. W. Ochterski, R. L. Martin, K. Morokuma, V. G. Zakrzewski, G. A. Voth, P. Salvador, J. J. Dannenberg, S. Dapprich, A. D. Daniels, Ö. Farkas, J. B. Foresman, J. V. Ortiz, J. Cioslowski, D. J. Fox, Gaussian, Inc., Wallingford CT, **2009**..

Received: April 27, 2013
Published online on ■■ ■■, 2013